

RESEARCH ARTICLE | SEPTEMBER 05 2024

Effect of width and thickness on propagating spin waves in permalloy microstripe waveguides

M. S. Devapriya ; Nair S. Aditya; Mahathi Kuchibhotla ; Adekunle Olusola Adeyeye ; Arabinda Haldar  

 Check for updates

J. Appl. Phys. 136, 093905 (2024)

<https://doi.org/10.1063/5.0223672>



View Online



Export Citation

Articles You May Be Interested In

Self-focusing of spin waves in Permalloy microstrips

Appl. Phys. Lett. (December 2007)

Spin wave wavevector up-conversion in Y-shaped Permalloy structures

Appl. Phys. Lett. (October 2021)

Localized parallel parametric generation of spin waves in a $\text{Ni}_{81}\text{Fe}_{19}$ waveguide by spatial variation of the pumping field

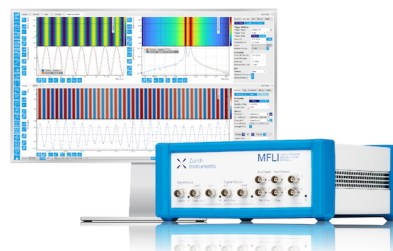
Appl. Phys. Lett. (March 2014)

Challenge us.

What are your needs for periodic signal detection?



Find out more



Effect of width and thickness on propagating spin waves in permalloy microstripe waveguides

Cite as: J. Appl. Phys. 136, 093905 (2024); doi: 10.1063/5.0223672

Submitted: 17 June 2024 · Accepted: 20 August 2024 ·

Published Online: 5 September 2024



M. S. Devapriya,¹  Nair S. Aditya,¹ Mahathi Kuchibhotla,¹  Adekunle Olusola Adeyeye,² 
and Arabinda Haldar^{1,a)} 

AFFILIATIONS

¹Department of Physics, Indian Institute of Technology Hyderabad, Kandi 502284, Telangana, India

²Department of Physics, Durham University, South Road, Durham DH1 3LE, United Kingdom

^{a)}Author to whom correspondence should be addressed: arabinda@phy.iith.ac.in

ABSTRACT

We report the effect of thickness and width on the spin wave transport and dispersion characteristics of permalloy (Py) microstripes using analytical calculations and experiments. Py waveguides with widths ranging from 2 to 4 μm were fabricated for two different thicknesses: 5 and 20 nm. Our results show a notable increase in the group velocity of spin waves with greater thickness, showing a fourfold rise as the thickness increases. Additionally, the accessible frequency range expands from 0.6 to 2.5 GHz as the thickness increases. We find that the spin wave mode frequency is affected by both thickness and width, with a frequency shift of approximately 0.2 GHz observed when the width increases from 2 to 4 μm . Moreover, spin waves decay more rapidly in thinner films, with the decay length of 20 nm-thick waveguides being four times longer than that of 5 nm-thick waveguides. Thicker and wider waveguides provide a longer decay length, facilitating the transmission of information over longer distances without significant energy loss. Our study offers an understanding of the spin wave propagation in microstrip waveguides and its potential in the development of future magnonic devices.

© 2024 Author(s). All article content, except where otherwise noted, is licensed under a Creative Commons Attribution-NonCommercial-NoDerivs 4.0 International (CC BY-NC-ND) license (<https://creativecommons.org/licenses/by-nc-nd/4.0/>). <https://doi.org/10.1063/5.0223672>

I. INTRODUCTION

Magnonics is an emerging research field focused on the transport and information processing of spin waves, which are collective excitations of electron spins in a magnetic material. One of the key challenges in developing magnonic devices is achieving efficient information transport using spin-based mechanisms. In metals, the high spin relaxation rate causes the information carried out by electron spin polarization to be lost within a few nanometers, making direct spin transport difficult. However, the recent discovery that spin wave-based spin currents are capable of information transport over long ranges has generated significant interest in the studies related to spin wave propagation.^{1–3} Magnonic devices have great potential to revolutionize Boolean^{4–6} and neuromorphic^{7,8} computing applications. These devices rely on waveguides for the propagation of spin waves. Waveguides based on metallic ferromagnetic films^{9–15} are widely used due to the ease of scaling them down to nanometer dimensions and integrating them with standard semiconductor technology.

The self-focusing effect¹⁶ in permalloy (Py) microstripe waveguides is an interesting phenomenon in spin wave propagation studies. Spin waves experience focusing at a specific distance from the excitation antenna, which is determined by the width of the wire. The quantization of several modes along the width of the microstripe and their copropagation can lead to interference effects. Consequently, this can cause periodic focusing and defocusing effects on spin waves along the axis of the stripe.¹⁷ The spin wave propagation can be well controlled by the modulation in width, thereby tuning the internal magnetic field. A spin wave can be split into two individual beams using a width-modulated stripe, which can be considered in developing a spin wave splitter.¹⁸ The phenomena such as spin wave lateral quantization and spin wave wells have also been reported in microstripe waveguides.^{19,20} There are also waveguide types that do not require any external bias magnetic field.^{21–24} Recent studies on thicker Py waveguides show that the decay length decreases with the increase in the thickness for thicknesses beyond 200 nm.²⁵ This is due to the additional damping induced by the electrical conductivity of metallic films.

31 October 2024 18:59:33

A width-dependent study on Py waveguides reveals that waveguides with a width $<5\ \mu\text{m}$ exhibit a rapid change in the intensity with the width due to the influence of shape anisotropy.²⁶ However, these studies are based on electrical measurements where magnons with very small wave vectors can be excited, as the antenna width is very large. Overall, past studies indicate that spin wave propagation is highly sensitive to the geometry of the waveguide, specifically its thickness and width. Although various research groups have investigated different geometries of Py micro-waveguide stripes, a systematic analysis of the combined influence of width and thickness on spin wave propagation is still lacking.

Here, we present a systematic study on the effect of the width and thickness of the Py microstripe waveguide on spin wave propagation using both analytical calculations and experiments. Py stripes of widths ranging from 2 to $4\ \mu\text{m}$ and thicknesses 5 and 20 nm were fabricated using lithography techniques. Spin waves were excited via a shorted coplanar waveguide (CPW) in Damon–Eshbach (DE) propagation geometry. We observed a significant increase in the group velocity of spin waves with an increase in the thickness of Py. Additionally, the spin wave mode frequencies increased due to the reduction in demagnetizing fields with greater width. Furthermore, we found that the decay length is sensitive to both thickness and width, with spin waves propagating over longer distances in wider, thicker waveguides.

II. METHODS

Figure 1(a) shows the schematic of the simplified micro-focused Brillouin light scattering (μ -BLS) experiment where a 532 nm laser (Spectra-Physics) beam is focused down to $\sim 250\ \text{nm}$ using a $\times 100$ objective with a large numerical aperture, $\text{NA} = 0.75$. The magnetic scattering beam from the waveguide is collected by the same objective and is directed to a multi-pass tandem Fabry–Pèrot interferometer (TFP-HC, JRS Scientific) for the detection of spin waves. A collinear white light and CCD camera setup are employed to visualize the sample and ensure the positional stability of the beam by measuring the reflected laser intensity from the waveguide using a feedback loop mechanism. Spin waves are excited by a shorted CPW connected to a frequency generator (Anritsu), which facilitates the excitation of spin waves in the micro-waveguides. The intensity of the BLS signal is proportional to the square of the dynamic magnetization under the laser spot. Further details of the μ -BLS experiment can be found elsewhere.²⁷ A uniform static field is applied along the width of the microstripes, satisfying the propagation geometry of the DE²⁸ spin waves. Spin waves in this geometry are width quantized and possess large group velocity.²⁹

The scanning electron microscopy (SEM) image of the sample, including the antenna, is shown in Fig. 1(b). Waveguides with two different thicknesses ($t = 5$ and $20\ \text{nm}$) were fabricated for three different widths ($w = 2, 3,$ and $4\ \mu\text{m}$). Additionally, $100\ \text{nm}$ -thick and $1\ \mu\text{m}$ -wide Au stripes were fabricated on top of the Py stripes. Py micro-waveguides and the narrower part of the excitation antenna are fabricated using the electron beam lithography technique followed by the lift-off process. The larger contact pad for the excitation antenna was fabricated using the photolithography technique. Note that Cr is used as a seed layer for the good adhesion of both Py and Au to the Si substrate. Py films were deposited using e-beam evaporation technique at a base pressure of 2×10^{-8} Torr.

III. RESULTS AND DISCUSSION

Figure 1(c) shows the spatial Fourier transform of the excitation field distribution of the antenna, given by, $h_{sK_x}(K_x) = \int_{-\infty}^{\infty} h_{sx}(x)\exp(iK_x x)dx$.³⁰ The function $|h_{sK_x}|$ exhibits a clear minimum at $K_x = \frac{2\pi}{d}$, where d is the width of the stripe antenna used. The excitation efficiency vanishes at this point.

The dispersion curves for spin waves propagating in Py stripes are calculated using the following equation:

$$\omega^2 = (\Omega_{\beta k} + \omega_M - \omega_M P_{\beta k})(\Omega_{\beta k} + \omega_M P_{\beta k} \sin^2 \phi), \quad (1)$$

where $\Omega_{\beta k} = \gamma H + \omega_M \alpha K_{\beta}^2$; $\omega_m = \gamma M_s$; and $K_{\beta}^2 = \kappa_{\beta}^2 + K_{\zeta}^2$. Here, γ is the gyromagnetic ratio, H is the applied external field, M_s is the saturation magnetization, α is the exchange constant, and K_{β} is the total spin wave vector. K_{β} has out-of-plane (κ_{β}) and in-plane (K_{ζ}) wave vector components. κ_{β} is quantized as $\kappa_{\beta} = \frac{\beta\pi}{t}$, where β is the quantization number along the thickness. On the other hand, K_{ζ} has components along the length (K_x) and width (K_w) directions. K_{ζ} can be expressed as $K_{\zeta}^2 = K_w^2 + K_x^2$. Note that K_w is quantized as $K_w = \frac{m\pi}{w}$, where m is the quantization number along the width. We have considered the most intense first-order mode, i.e., $m = 1$. ϕ is the angle between H and K_{ζ} . The expansion of polynomial $P_{\beta k}$ and detailed derivation of these expressions can be found elsewhere.^{31–33} Standard parameters of Py are used for calculations: $M_s = 8 \times 10^5\ \text{A/m}$ and $\alpha = 13 \times 10^{-12}\ \text{J/m}$. Figure 2(a) describes the spin wave dispersion relation of 5 nm-thick Py microstripes for various widths at 110 mT. The dotted lines correspond to the limit of antenna excitation efficiency. The inset represents a zoomed-in view of the region near zero in the dispersion curve. It is found that the slope of the curve for wider stripes increases at a higher rate in this region. A similar plot of the dispersion curve for Py stripes of various widths, with a thickness of 20 nm, is shown in Fig. 2(b). One may notice a slight increase in the cut-off frequency (at $K_x = 0$) when the waveguide width is increased from 2 to $4\ \mu\text{m}$ for a 5 nm-thick waveguide. This shift is attributed to the decreasing demagnetizing field along the width as the width increases, leading to a larger effective internal field along the width. The cut-off frequencies exhibit a more prominent shift with the width for higher thickness. It increases from 9.4 to 9.6 GHz with the width. Note that the external field is applied along the width of the waveguides. On the other hand, for a given waveguide width, the cut-off frequency is slightly smaller for the thicker waveguide. It follows from the fact that the demagnetization field along the thickness decreases with increasing thickness, which results in a larger demagnetization field along the width, leading to a reduced effective internal field along the width. The figure clearly shows that an increase in the thickness significantly alters the dispersion curve. Specifically, the slope of the curve, or the group velocity (v_g), sharply increases with greater thickness. Consequently, the range of accessible frequencies also expands. For a 5 nm-thick and $2\ \mu\text{m}$ -wide stripe, the accessible frequency range is between 9.7 and 10.3 GHz. In contrast, for a 20 nm-thick and $2\ \mu\text{m}$ -wide stripe, the range extends from 9.4 to 11.5 GHz. It is also to be noted that the cut-off frequencies for a particular width have decreased with increasing thickness. The calculated v_g of the spin waves as a

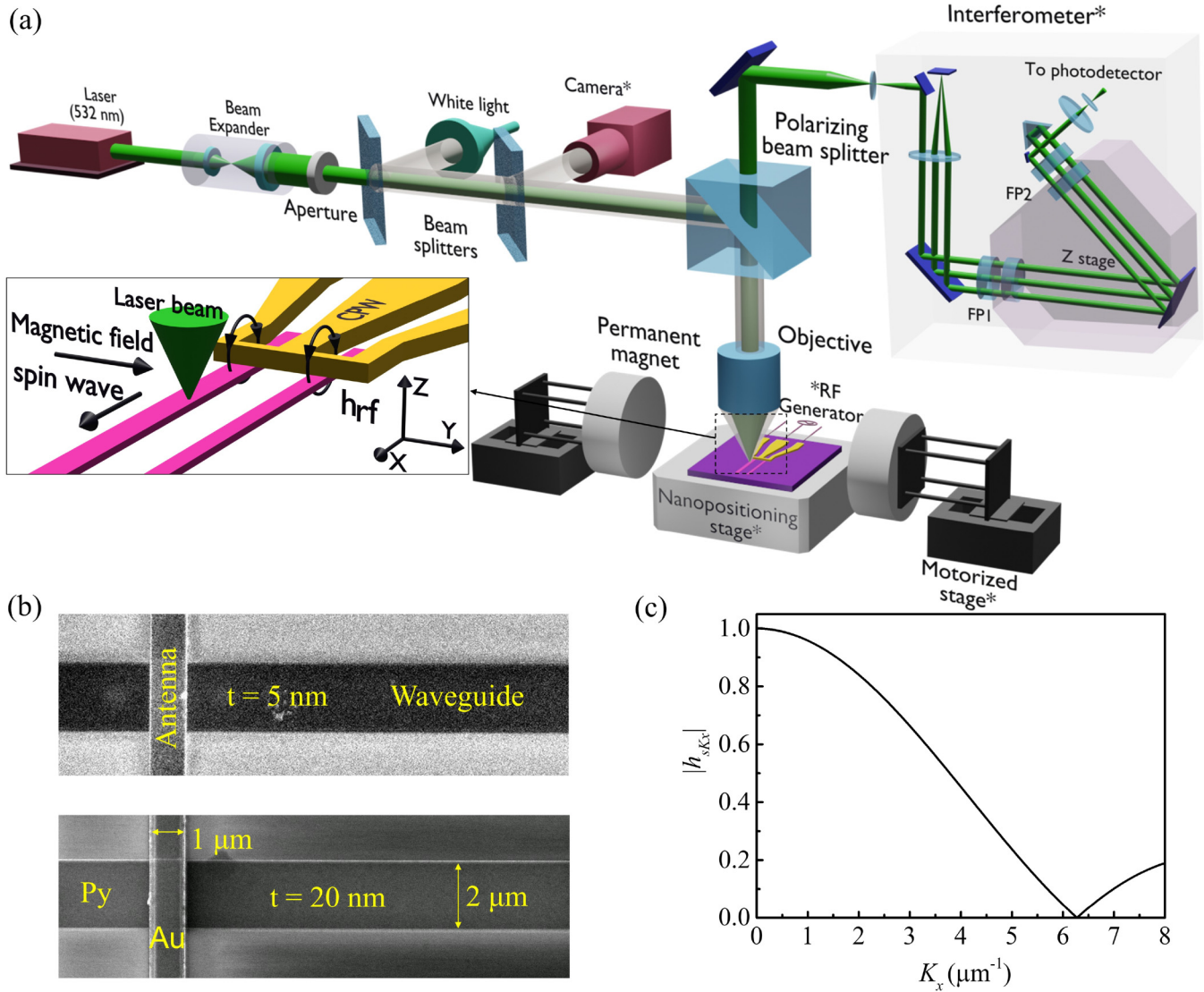


FIG. 1. (a) Schematic of the μ -BLS experiment. The incoming laser beam is focused using a $\times 100$ objective onto the sample placed on a nanostaging stage. A magnetic field is applied along the Y-axis. Spin waves are excited using a shorted CPW, which is connected to an RF signal generator. The scattered beam from the sample is fed to the interferometer with the help of a polarizing beam splitter. A colinear arrangement of the camera and white light is used for visualization and stabilization. The components marked with an asterisk are connected to the computer. A zoomed-in view of the sample indicates the direction of the RF field, applied magnetic field, and propagating spin waves. (b) SEM image of the sample along with the excitation antenna. (c) Spatial Fourier transform of the antenna field normalized with respect to that at $K_x = 0$.

function wave vector for different width at $t = 5$ nm and $t = 20$ nm is plotted in Figs. 2(c) and 2(d), respectively. v_g is calculated using the equation given by

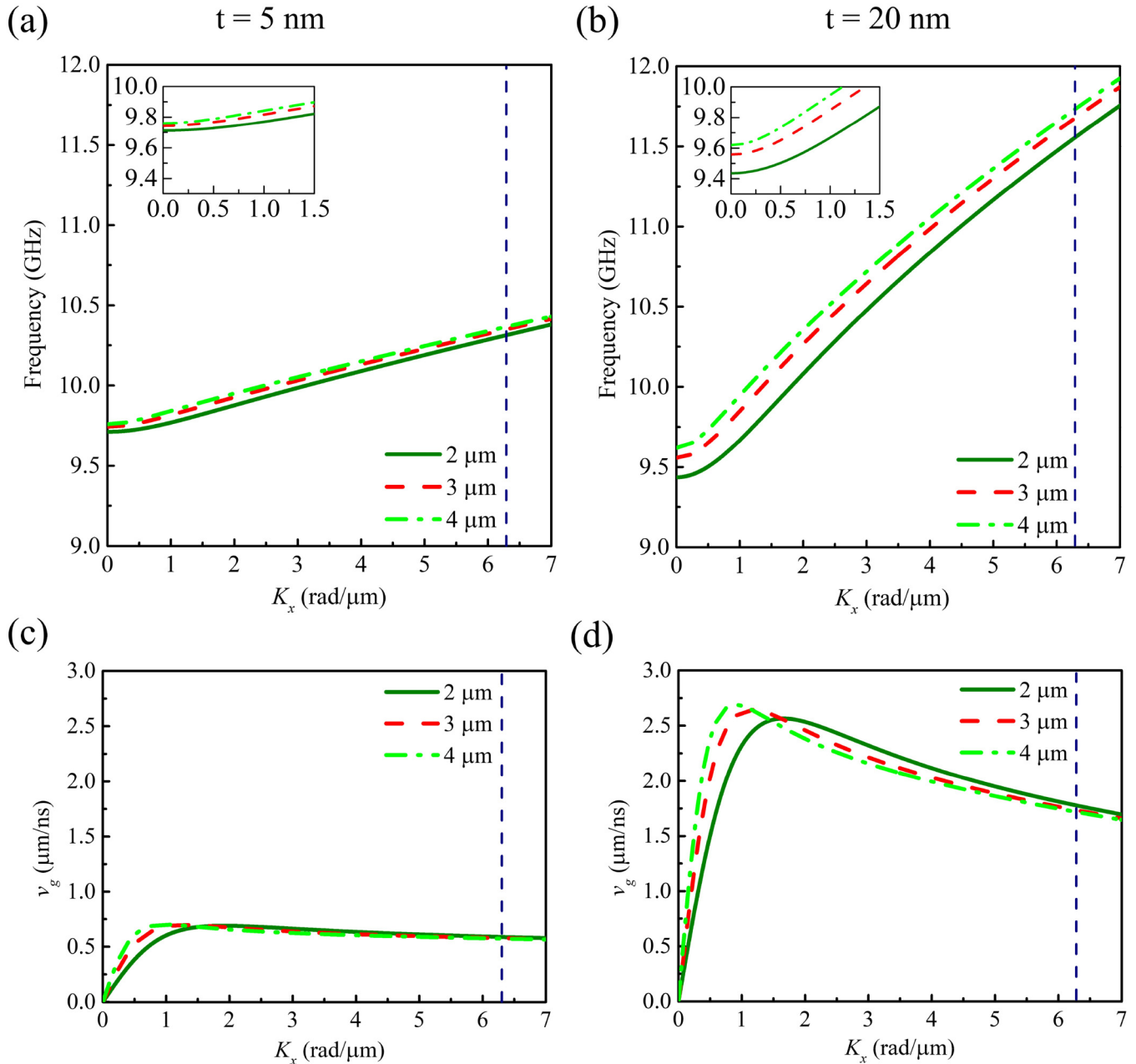
$$v_g = \frac{\partial \omega}{\partial K_x}. \quad (2)$$

It is evident from the figure that the v_g of the spin waves exhibits a notable increase with the thickness. The v_g of the wires

increases fourfold when the thickness increases from 5 to 20 nm. v_g also shows an increasing trend with the width for both the thicknesses up to a certain wave vector, beyond which it decreases.

These interesting features in the spin wave dispersion relation led us to carry out a detailed experimental analysis of the effect of width and thickness on the Py waveguides. The 2D BLS spectra of the 5 nm-thick Py waveguide for various widths are shown in Fig. 3(a). The stripe was initially saturated at a higher field, and BLS spectra were acquired for magnetic fields ranging from 220 to

31 October 2024 18:59:33



31 October 2024 18:59:33

FIG. 2. Dispersion characteristics of the first-order spin wave modes for various widths of stripes for thickness (a) 5 and (b) 20 nm at 110 mT. The calculated group velocity of first-order spin wave modes for various widths of stripes and thicknesses (c) 5 and (d) 20 nm at 110 mT. The dotted lines indicate the cut-off wave vector corresponding to the excitation antenna.

20 mT with a step of 10 mT by sweeping the frequency from 3 to 20 GHz in a step of 0.5 GHz. The spectra were measured with the laser spot positioned 1 μm away from the excitation antenna, approximately in the middle of the stripe. The intensity of the

inelastic signal was normalized against the elastic signal to account for any fluctuations in laser intensity. We observe a clear increase in the intensity of the spectra with increased thickness. The normalized BLS spectra for 5 nm-thick Py stripe, for various widths at

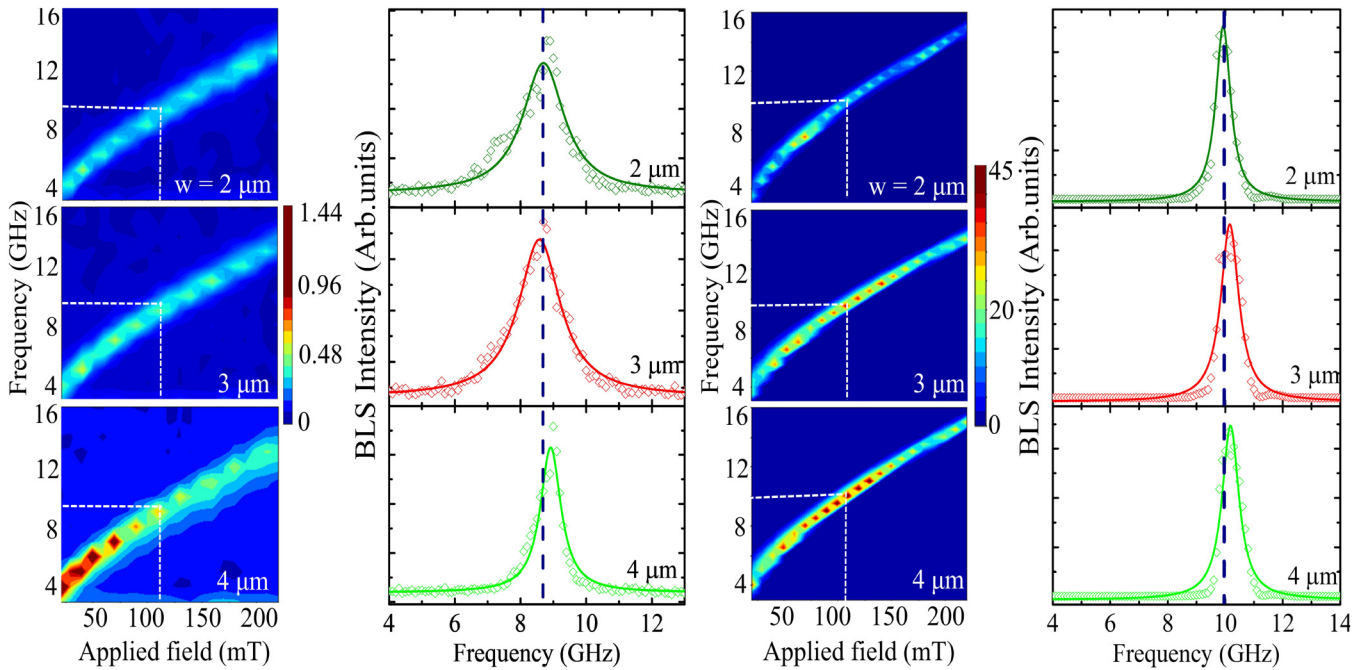


FIG. 3. 2D BLS spectra of microstrips with varying width for thicknesses (a) 5 and (c) 20 nm. The color bar indicating the intensity of the BLS signal is given adjacent to the plots. The normalized BLS spectra at 110 mT for thicknesses (b) 5 and (d) 20 nm, with variable width. The solid lines represent fit to the experimental data using a Lorentzian function.

110 mT, are shown in Fig. 3(b). The experimental data were fitted using a Lorentzian curve, and the peaks exhibited a slight shift toward higher frequencies with increasing width. The frequency increased from 8.7 to 8.9 GHz as the width varied from 2 to 4 μm. This shift is attributed to the changes in the internal field. As the width increases, the demagnetizing field associated with the microstrip decreases, resulting in a higher frequency. It is also to be noted that the linewidth of the peak decreases with increasing width. A similar plot showing the variation in the width for 20 nm-thick stripes is shown in Fig. 3(d). The FWHM calculated from the Lorentzian fit reveals that the linewidth decreases from 1.5 to 0.8 GHz as the width increases from 2 to 4 μm for 5 nm-thick microstrips. However, the linewidth variation with width is insignificant for a 20 nm-thick microstrip waveguide. The spin wave mode frequency is almost 1 GHz higher when the thickness is increased from 5 to 20 nm. Additionally, the BLS intensity is one order of magnitude higher for the 20 nm-thick waveguides.

Decay length is a crucial factor in spin wave-based applications as it determines the distance over which information can be transferred without significant energy loss. The stripes were excited at their corresponding resonance frequencies for 110 mT, and the laser spot was scanned along the middle of the stripe up to a length of 8 μm in 0.1 μm step. The position of the wire close to the antenna is defined as $x=0$. Spatial decay of the spin waves along the 5 nm-thick and 20 nm-thick waveguides for various widths is shown in Figs. 4(a) and 4(b). It can be observed that the intensity

of spin waves decays significantly within a short distance from the antenna in the 5 nm-thick stripes, whereas this decay is more gradual in 20 nm-thick waveguides. The slight irregularities close to the excitation antenna for 20 nm-thick waveguides can be attributed to the interference of multiple modes.

The decay characteristic can be fitted with the following exponential function:

$$I(x) = Ae^{-\frac{x}{\lambda_D}} + I_0, \quad (3)$$

where x is the propagation coordinate, $I(x)$ is the intensity obtained from experiments, λ_D is the decay length, and I_0 is the offset. The decay length obtained from the fit for both the thickness as a function of width is plotted in Fig. 4(c). The decay length slightly increases with width in both cases. Additionally, the decay length is more than tripled with the increase in the thickness, which can be attributed to the significant increase in the group velocity of spin waves with the thickness as observed from the dispersion curve, as shown in Figs. 2(c) and 2(d). We have also calculated the decay length of the microstrip using the following equation:

$$\lambda_D = \frac{v_g}{2\alpha_G\omega}, \quad (4)$$

where α_G is the Gilbert damping parameter and ω is the spin wave frequency. The open symbols in Fig. 4 represent the calculated

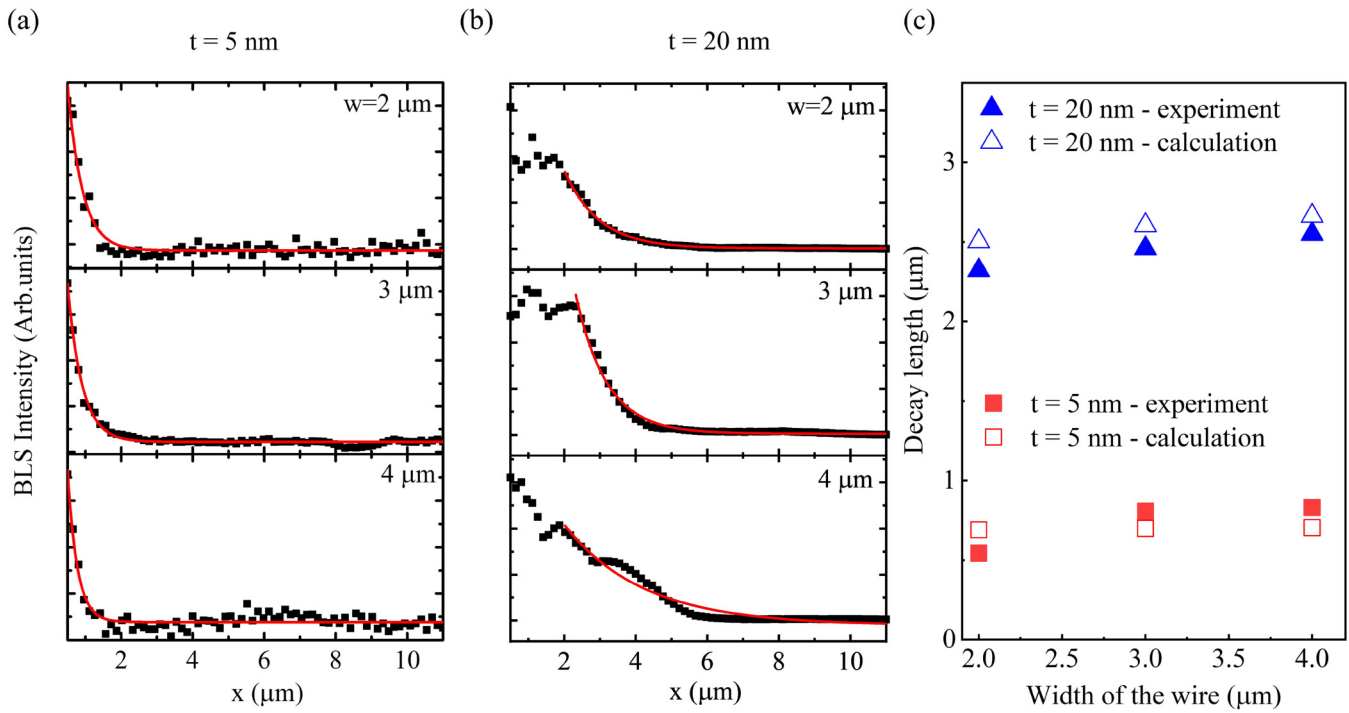


FIG. 4. Spin wave intensity plotted against the propagation distance for thicknesses (a) 5 and (b) 20 nm for various widths. The solid lines represent an exponential fit to the experimental data. (c) The calculated decay length is a function of width of the microstrip for different thicknesses. The open symbols represent the decay length obtained from analytical calculations, and the solid symbols represent the decay length obtained from experiments.

31 October 2024 18:59:33

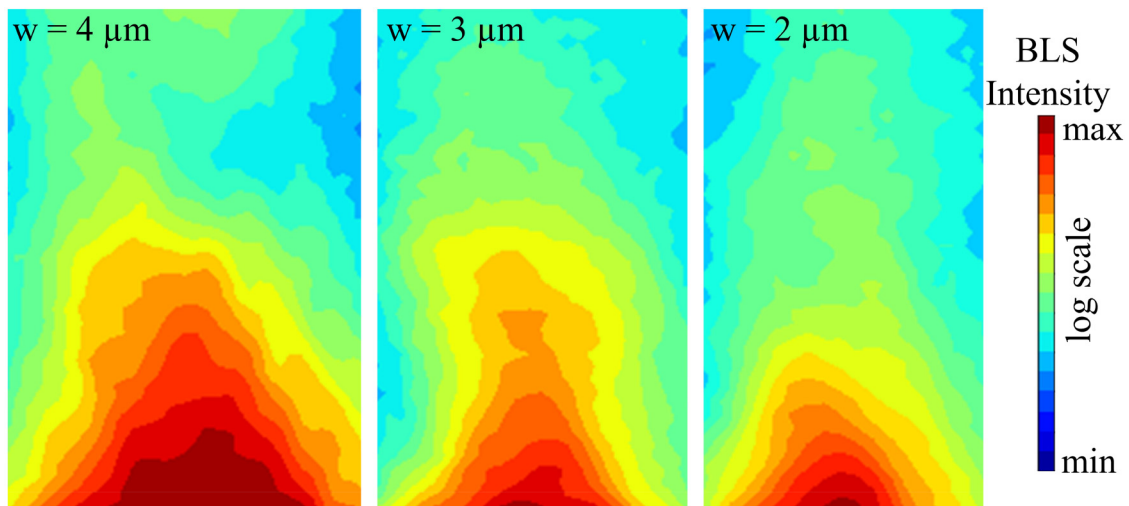


FIG. 5. 2D map of spin wave intensity obtained from space resolved measurements for microstrips of various widths and thickness 20 nm, carried out at 110 mT. Blue color corresponds to the minimum, and red color to the maximum BLS intensity. The plots are on a logarithmic scale.

decay length values. The experimental results agree with the calculated decay length values.

To gain further insight into spin wave propagation, a 2D μ -BLS image was acquired for all the samples (Fig. 5). The laser spot was scanned over an $8\ \mu\text{m}$ length range in 200 nm steps along the length and 100 nm steps along the width of the stripe. Measurements were conducted at $\mu_0 H = 110\ \text{mT}$ and the corresponding frequencies with maximum intensity [as in Fig. 3(c)] for each width, i.e., frequency, $f = 9.9, 10.1,$ and $10.2\ \text{GHz}$ for $w = 2, 3,$ and $4\ \mu\text{m}$, respectively. The plots are presented on a logarithmic scale. The decay is not uniform along the width of the stripe when moving away from the antenna. The decay rate is very high at the edges when compared to the middle of the stripe. This shaped beam can be a result of the focusing effect on the stripes and energy dissipation.¹⁶ It is also evident from the figures that the spin wave propagates to a farther distance with the increase in the width. This is consistent with the analytical predictions as shown in Figs. 2(a)–2(d).

IV. CONCLUSION

To summarize, we have conducted a systematic, comprehensive investigation on the effect of the thickness and width of the Py microstripe waveguides on the spin propagation characteristics. Py microstrips of width 2, 3, and $4\ \mu\text{m}$ were fabricated for two thicknesses: 5 and 20 nm. Spin waves were directly probed using the μ -BLS technique. Analytical studies revealed a substantial increase in the group velocity of spin waves with increased waveguide thickness. The group velocity increased fourfold with the thickness. Additionally, the range of accessible frequencies increased with thickness. The accessible frequency range for a 5 nm-thick and $2\ \mu\text{m}$ -wide stripe was 0.6 GHz, whereas it was 2.1 GHz for a 20 nm-thick and $2\ \mu\text{m}$ -wide stripe. The frequency of the spin wave mode was also found to be sensitive to the width of the microstripe due to changes in the demagnetizing fields within the stripe, with a 0.2 GHz increase observed when the width was varied from 2 to $4\ \mu\text{m}$. Furthermore, the spin wave intensity increased significantly with thickness by an order of magnitude. The decay length was found to be tunable by changing the width and thickness of the waveguide. The decay length of the 20 nm-thick waveguide was four times that of the 5 nm-thick waveguide, suggesting that spin waves in thicker and wider waveguides can propagate longer distances. Our findings offer valuable insights into fundamental aspects of spin wave propagation in microstripe waveguides and have important implications for future magnonic devices.

ACKNOWLEDGMENTS

A.H. acknowledges the funding under the Core Research Grant (No. CRG/2022/004492), Science and Engineering Research Board (SERB), India. A.O.A. acknowledges the funding from the Royal Society and Wolfson Foundation.

AUTHOR DECLARATIONS

Conflict of Interest

The authors have no conflicts to disclose.

Author Contributions

M. S. Devapriya: Data curation (equal); Formal analysis (equal); Investigation (equal); Methodology (equal); Writing – original draft (lead). **S. Nair Aditya:** Data curation (equal); Investigation (equal); Methodology (equal). **Mahathi Kuchibhotla:** Data curation (equal); Investigation (equal); Methodology (equal). **Adekunle Olusola Adeyeye:** Conceptualization (equal); Funding acquisition (equal); Investigation (equal); Project administration (equal); Supervision (equal); Writing – review & editing (equal). **Arabinda Haldar:** Conceptualization (equal); Funding acquisition (equal); Investigation (equal); Project administration (equal); Supervision (equal); Writing – review & editing (equal).

DATA AVAILABILITY

The data that support the findings of this study are available within the article.

REFERENCES

- V. V. Kruglyak, S. O. Demokritov, and D. Grundler, “Magnonics,” *J. Phys. D: Appl. Phys.* **43**(26), 264001 (2010).
- A. V. Chumak, V. I. Vasyuchka, A. A. Serga, and B. Hillebrands, “Magnon spintronics,” *Nat. Phys.* **11**(6), 453–461 (2015).
- B. Lenk, H. Ulrichs, F. Garbs, and M. Münzenberg, “The building blocks of magnonics,” *Phys. Rep.* **507**(4–5), 107–136 (2011).
- T. Goto, T. Yoshimoto, B. Iwamoto, K. Shimada, C. A. Ross, K. Sekiguchi, A. B. Granovsky, Y. Nakamura, H. Uchida, and M. Inoue, “Three port logic gate using forward volume spin wave interference in a thin yttrium iron garnet film,” *Sci. Rep.* **9**(1), 16472 (2019).
- G. Talmelli, T. Devolder, N. Träger, J. Förster, S. Wintz, M. Weigand, H. Stoll, M. Heyns, G. Schütz, I. P. Radu, J. Gräfe, F. Ciubotaru, and C. Adelmann, “Reconfigurable submicrometer spin-wave majority gate with electrical transducers,” *Sci. Adv.* **6**(51), 4042–4060 (2020).
- T. Fischer, M. Kewenig, D. A. Bozhko, A. A. Serga, I. I. Syvorotka, F. Ciubotaru, C. Adelmann, B. Hillebrands, and A. V. Chumak, “Experimental prototype of a spin-wave majority gate,” *Appl. Phys. Lett.* **110**(15), 152401 (2017).
- T. Brächer and P. Pirro, “An analog magnon adder for all-magnonic neurons,” *J. Appl. Phys.* **124**(15), 152119 (2018).
- A. Papp, W. Porod, and G. Csaba, “Nanoscale neural network using non-linear spin-wave interference,” *Nat. Commun.* **12**(1), 6422 (2021).
- S. Choi, K. S. Lee, K. Y. Guslienko, and S. K. Kim, “Strong radiation of spin waves by core reversal of a magnetic vortex and their wave behaviors in magnetic nanowire waveguides,” *Phys. Rev. Lett.* **98**(8), 087205 (2007).
- A. Haldar and A. O. Adeyeye, “Functional magnetic waveguides for magnonics,” *Appl. Phys. Lett.* **119**(6), 060501 (2021).
- R. Hertel, W. Wulfhekel, and J. Kirschner, “Domain-wall induced phase shifts in spin waves,” *Phys. Rev. Lett.* **93**(25), 257202 (2004).
- T. Sebastian, Y. Ohdaira, T. Kubota, P. Pirro, T. Brächer, K. Vogt, A. A. Serga, H. Naganuma, M. Oogane, Y. Ando, and B. Hillebrands, “Low-damping spin-wave propagation in a micro-structured $\text{Co}_2\text{Mn}_{0.6}\text{Fe}_{0.4}\text{Si}$ Heusler waveguide,” *Appl. Phys. Lett.* **100**(11), 112402 (2012).
- A. I. Nikitchenko and N. A. Pertsev, “Spin-orbit torque control of spin waves in a ferromagnetic waveguide,” *Phys. Rev. B* **104**(13), 134422 (2021).
- V. E. Demidov, S. O. Demokritov, K. Rott, P. Krzysteczko, and G. Reiss, “Nano-optics with spin waves at microwave frequencies,” *Appl. Phys. Lett.* **92**(23), 232503 (2008).
- M. P. Kostylev, G. Gubbiotti, J. G. Hu, G. Carlotti, T. Ono, and R. L. Stamps, “Dipole-exchange propagating spin-wave modes in metallic ferromagnetic stripes,” *Phys. Rev. B* **76**(5), 054422 (2007).

- ¹⁶V. E. Demidov, S. O. Demokritov, K. Rott, P. Krzysteczko, and G. Reiss, "Self-focusing of spin waves in permalloy microstrips," *Appl. Phys. Lett.* **91**(25), 252504 (2007).
- ¹⁷V. E. Demidov, S. O. Demokritov, K. Rott, P. Krzysteczko, and G. Reiss, "Mode interference and periodic self-focusing of spin waves in permalloy microstrips," *Phys. Rev. B* **77**(6), 064406 (2008).
- ¹⁸V. E. Demidov, J. Jersch, S. O. Demokritov, K. Rott, P. Krzysteczko, and G. Reiss, "Transformation of propagating spin-wave modes in microscopic waveguides with variable width," *Phys. Rev. B* **79**(5), 054417 (2009).
- ¹⁹J. Jorzick, S. O. Demokritov, C. Mathieu, B. Hillebrands, B. Bartenlian, C. Chappert, F. Rousseaux, and A. N. Slavin, "Brillouin light scattering from quantized spin waves in micron-size magnetic wires," *Phys. Rev. B* **60**(22), 15194–15200 (1999).
- ²⁰J. Jorzick, S. O. Demokritov, B. Hillebrands, M. Bailleul, C. Fermon, K. Y. Guslienko, A. N. Slavin, D. V. Berkov, and N. L. Gorn, "Spin wave wells in nonellipsoidal micrometer size magnetic elements," *Phys. Rev. Lett.* **88**(4), 4 (2002).
- ²¹K. O. Nikolaev, S. R. Lake, G. Schmidt, S. O. Demokritov, and V. E. Demidov, "Zero-field spin waves in YIG nanowaveguides," *Nano Lett.* **23**(18), 8719–8724 (2023).
- ²²A. Haldar, C. Tian, and A. O. Adeyeye, "Isotropic transmission of magnon spin information without a magnetic field," *Sci. Adv.* **3**(7), e1700638 (2017).
- ²³A. Haldar, D. Kumar, and A. O. Adeyeye, "A reconfigurable waveguide for energy-efficient transmission and local manipulation of information in a nano-magnetic device," *Nat. Nanotechnol.* **11**(5), 437–443 (2016).
- ²⁴K. Wagner, A. Kákay, K. Schultheiss, A. Henschke, T. Sebastian, and H. Schultheiss, "Magnetic domain walls as reconfigurable spin-wave nanochannels," *Nat. Nanotechnol.* **11**(5), 432–436 (2016).
- ²⁵T. Manago, M. M. Aziz, F. Ogrin, and K. Kasahara, "Influence of the conductivity on spin wave propagation in a permalloy waveguide," *J. Appl. Phys.* **126**(4), 043904 (2019).
- ²⁶K. Kasahara, R. Akamatsu, and T. Manago, "Ferromagnetic-waveguide width dependence of propagation properties for magnetostatic surface spin waves," *AIP Adv.* **11**(4), 045308 (2021).
- ²⁷S. O. Demokritov and V. E. Demidov, "Micro-Brillouin light scattering spectroscopy of magnetic nanostructures," *IEEE Trans. Magn.* **44**(1), 6–12 (2008).
- ²⁸R. W. Damon and J. R. Eshbach, "Magnetostatic modes of a ferromagnet slab," *J. Phys. Chem. Solids* **19**(3–4), 308–320 (1961).
- ²⁹S. Urazhdin, V. E. Demidov, H. Ulrichs, T. Kendziorczyk, T. Kuhn, J. Leuthold, G. Wilde, and S. O. Demokritov, "Nanomagnonic devices based on the spin-transfer torque," *Nat. Nanotechnol.* **9**(7), 509–513 (2014).
- ³⁰V. E. Demidov, M. P. Kostylev, K. Rott, P. Krzysteczko, G. Reiss, and S. O. Demokritov, "Excitation of microwaveguide modes by a stripe antenna," *Appl. Phys. Lett.* **95**(11), 112509 (2009).
- ³¹B. A. Kalinikos, "Excitation of propagating spin waves in ferromagnetic films," in *IEE Proceedings H Microwaves, Optics and Antennas* (1980), Vol. 127(1), p. 4.
- ³²B. A. Kalinikos and A. N. Slavin, "Theory of dipole-exchange spin wave spectrum for ferromagnetic films with mixed exchange boundary conditions," *J. Phys. C: Solid State Phys.* **19**, 7013–7033 (1986).
- ³³D. N. Chartoryzhskii, B. A. Kalinikos, and O. G. Vendik, "Parallel pump spin wave instability in thin ferromagnetic films," *Solid State Commun.* **20**(10), 985–989 (1976).